Article

Not peer-reviewed version

Accelerated Refueling of Type IV Hydrogen Pressure Tanks by Passive Means: Thermal Material Characterization and Evaluation

Nico Liebers * and Sven Ropte †

Posted Date: 4 March 2026

doi: 10.20944/preprints202603.0319.v1

Keywords: composite manufacturing; hydrogen pressure vessel; thermal management; thermal conductivity

 doi:10.20944/preprints202603.0319.v1

Article

Accelerated Refueling of Type IV Hydrogen Pressure Tanks by Passive Means: Thermal Material Characterization and Evaluation

Nico Liebers * and Sven Ropte †

German Aerospace Center (DLR), Institute of Lightweight Structures
* Correspondence: nico.liebers@dlr.de
† Current address: Lilienthalplatz 7, 38108 Braunschweig, Germany

Abstract

The significant heat generation during refueling of hydrogen pressure tanks might exceed the permissible 85 °C temperature limit for type IV tanks consisting of a thermoplastic liner and a carbon fiber composite overwrap. Common countermeasures like hydrogen pre-cooling or long filling times are energy and time consuming, hence in this paper passive means through thermally better suited materials are examined. Therefore state of the art and alternative materials are first characterized and finally compared using a transient heat model. The different material combinations are compared for maximum temperature and weight in a typical filling scenario. As alternative liner materials thermoplastics filled with short carbon fibres, minerals and graphite and concerning the composite overwrap copper coated carbon fibres were chosen to improve thermal properties. The findings show that the liner is the bottleneck while transferring heat from the inner to the outer tank surface. Using graphite filled thermoplastic as liner material shows the highest potential regarding thermal optimization with only little weight increase. Using additionally copper coated carbon fibres reduces the maximum temperature further, but at a high weight increase. This article is a revised and expanded version of a paper, which was presented at the 15th EASN International Conference, in Madrid, Spain, in October 2025 [1].

Keywords: composite manufacturing; hydrogen pressure vessel; thermal management; thermal conductivity

1. Introduction

Hydrogen is one of the emerging renewable energy carrier options as the refueling consumes less time than recharging batteries. For mobile applications pressurized hydrogen tanks are widely used due to their technical maturity, robustness and cost advantages. [2–5]

Hydrogen pressure tanks can be classified into Types I to V as shown in Figure 1. Type I corresponds to an all-metal tank, Type II is a metallic tank with carbon fibre reinforced plastic (CFRP) overwrap in the cylindrical area. Type III and IV consist of a complete composite overwrap with a metallic and a thermoplastic liner respectively. Type V tank is an only composite tank, but is still technologically not yet mature and the focus of development. [4,6]

The gravimetrical storage capacity and storage pressure increase from Type I to Type IV, hence Type IV is the most used pressure storage in mobile applications [6]. The thermoplastic liner – commonly PA or HDPE – is used as the mandrel the during manufacturing by fibre winding and then acts as the hydrogen permeation barrier and contributes only marginally to the mechanical strength [6]. While the thermoplastic liner of Type IV tanks leads to better fatigue resistance, hydrogen permeability is higher and thermal conductivity – the focus of this paper – is lower than those of metallic liners of Type III tanks.

 doi:10.20944/preprints202603.0319.v1

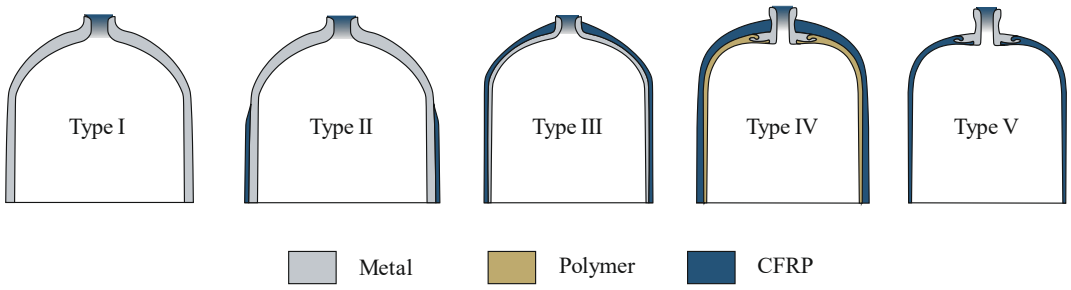

Figure 1. Pressure tank types I to V [7]

During refueling of hydrogen into the pressure tanks a significant quantity of heat is released due to friction of high flow, the Joules Thompson effect and compression work [8,9], which then is transferred into the tank structure. Standards exist for automobile applications [10,11], where the temperature rise must not exceed 85 °C. Hence, for fast refueling it is often necessary to use countermeasures, like pre-cooling of the hydrogen, multi-stage fills with lower fill rates at the beginning to reduce flow velocities and also active cooling of the structure . These measures lead to more energy consumption, cost and might increase filling duration. Additionally filling can only take place until the storage pressure is reached after which the gas cools down while pressure falls, so the intended state of charge (SOC) is not reached. [9,12–15]

Therefore improving the thermal properties - e.g. thermal conductivity and heat capacity - of the tank structure is desired and the aim of this paper. There are numerous publications on the thermal aspect of refueling Type II and IV tanks, many focus on complex CFD real-gas simulations, often using material properties from literature. Heat development and distribution depend strongly on tank, nozzle and general fuelling geometry and also on fill rate and other parameters. [9,12–18]

A promising approach is to use filled thermoplastics as liner material, which was examined in a PhD thesis by Rosen [4] in the context of Type IV tanks for automobile applications. Not only the thermal conductivity but also the hydrogen permeability can be improved by fillers. The enhanced thermal conductivity of thermoplastics by adding fillers is the focus of numerous publications [19–25].

To improve the heat transfer through the composite overwrap, copper coated carbon fibres show a lot of potential. Also nickel coated carbon fibres or modification of the thermoset matrix are possible measures to improve thermal conductivity, but the copper coating shows highest effect. [26,27]

2. Materials and Methods

In order to analyze and improve the heat transfer through the tank structure the commonly used and potentially better suited materials are characterized for density, filler content, fibre volume content, heat capacity, thermal conductivity (out-of-plane) and temperature diffusivity (in- and out-of-plane). The gained material properties were used to model the transient heat transfer through the tank structure during refueling and to compare different material combinations and hence find better suited materials regarding thermal performance.

In Table 1 the evaluated materials are listed starting with different polyamides (PA) and HDPE as commonly used liner materials. Different commercially available polyamides filled with short carbon fibres (CF), mineral fillers and graphite were analyzed as thermally better suited liner materials. Regarding the composite overwrap a reference material and a composite material made from copper coated carbon fibres (ccCFRP) were examined. The sample names of the filled thermoplastics include the gravimetric filler content derived from density measurements (see Section 3.1.2).

 doi:10.20944/preprints202603.0319.v1

Table 1. List of examined thermoplastic materials.

Sample Name	Manufacturer or Seller	Commercial Name	Description
PA6_1	Erwin Telle GmbH	Polyamid Guss PA 6 G	molded PA6
PA6_2		Polyamid extrudiert PA 6	extruded PA6
PA12		Polyamid PA 12	PA 12
HDPE	Reichelt Chemietechnik	-	HDPE
PA12_8%CF	n.a.[1]	n.a.[1]	PA12 with 8% carbon fibre
PA12_15%CF			PA12 with 15% carbon fibre
PA12_30%CF			PA12 with 30% carbon fibre
PA6_Mineral	MOCOM ALCOM	TCD PA6 5060 FR 16089	PA6 with high mineral filler content
PA66_17%Graphite		PA66 910/32.1 TCE2 BK1282-10	PA66 with graphite filler[2]
PA66_GF_42%Graphite		PA66 910/32.1 GF8 TCE8	PA66 with glass fibre and high graphite filler content[2]
CFRP	Toho Tenax	HTS 5631 800tex 12k	Composite reference (with resin below)
ccCFRP	Inca Fibre	*Mitsubishi Grafil 34-700* with 0.5µm copper coating[3]	Copper coated composite (with resin below)
Resin	SICOMIN	SR1710 (resin) and SD8822 (hardener)	Used for CFRP and ccCFRP

[1] Publication of brand name not permitted by manufacturer. [2] Presumably carbon black. [3] Due to time schedule issues, only remaining stock material could be used with uneven coating.

2.1. Preparation of Composite Samples

To analyse the composite materials, samples had to be prepared from the fibre material available as rovings. Using a fibre winding process the rovings were placed unidirectional on a steel drum with a diameter of 600 mm (see Figure 2) and manually impregnated with resin using a brush. Both composite material samples, the reference and the copper coated rovings, were prepared at the same time using the same procedure. Afterward the layup was cut, taken from the drum, cut into eight quadratic cutouts and stacked into a layup $[0°,\ 90°]_{4s}$. Curing occured under a vacuum bagging using a caul plate first under room ambience for 24 hours and then in an oven at 80 $°C$ for 8 hours.

 doi:10.20944/preprints202603.0319.v1

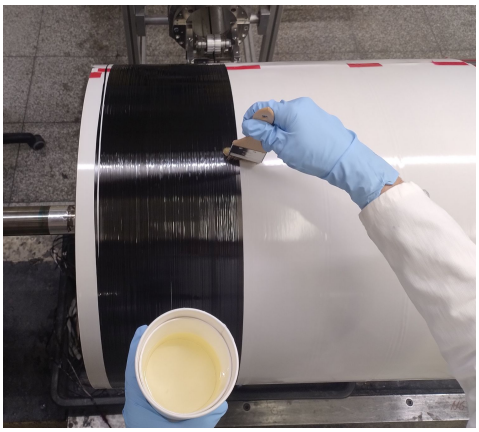

(a)

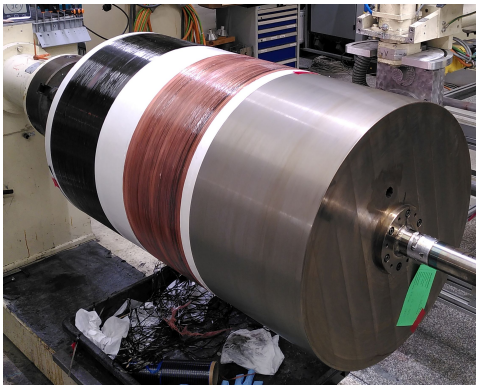

(b)

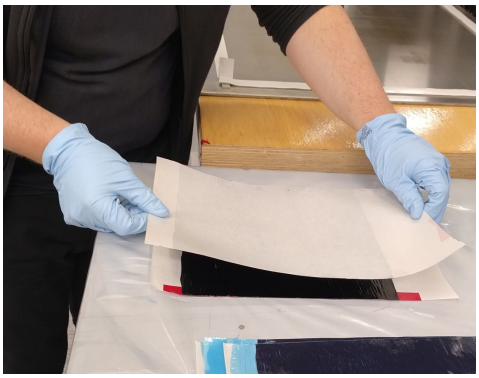

(c)

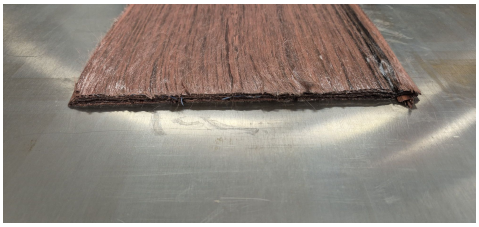

(d)

Figure 2. Preparation of composite samples by fiber winding: (**a**) Manual impregnation of fibers using brush. (**b**) Fibre winding of carbon fibre and copper coated carbon fiber on drum. (**c**) Layup after cutting. (**d**) Finished layup of copper coated fiber.

3. Results

3.1. Material Characterization

3.1.1. Fibre Volume Content

The two composite samples CFRP and ccCFRP manufactured as described above were analyzed for their fibre volume content by thermogravimetric analysis (TGA) following ISO11385 using a *Mettler Toledo TGA/DSC 3+*. The TGA started with drying the samples at 120 °C for 120 min under nitrogen atmosphere after which the dry mass m_{tot} was measured. After that the samples were continuously heated at 10 $K \cdot min^{-1}$ in an oxygen atmosphere to 450 °C and remained for 230 min at that temperature removing the thermoset matrix and acquire the mass of the fibres m_F. The fibre ϱ_F and sample densities ϱ_{tot} were measured using the buoyancy principle (see Section 3.1.2). The fibre volume content is calculated by:

$$\Phi = \frac{V_F}{V_{tot}} = \frac{m_F \cdot \varrho_{tot}}{\varrho_F \cdot m_{tot}} \tag{1}$$

The results are listed in Table 2. Concerning the reference CFRP sample the achieved FVC of 48.6% is acceptable, but for the ccCFRP sample the FVC of 27.8% is too low. The reasons for the low FVC are assumed to be that the excessive resin could not bleed out due to blocked flow paths, lack of absorption material and too low pressure during cure under vacuum. The ccCFRP samples have been used for material characterizations, but for comparing different materials in the thermal simulation part, values published by Bard [26,27] were used. Due to the time schedule the sample preparation could not be repeated.

 doi:10.20944/preprints202603.0319.v1

Table 2. Results of fibre volume measurement.

Sample	ϱ_{tot} $\left[\frac{kg}{m^3}\right]$	m_{tot} $[mg]$	ϱ_F $\left[\frac{kg}{m^3}\right]$	m_F $[mg]$	Φ_F [%]	$\bar{\Phi}_F \pm \sigma$ [%]
CFRP	1432	135.89	1780	81.37	47.9	48.6 ± 0.48
	1438	135.06		83.57	49.0	
	1444	139.38		84.41	48.9	
ccCFRP	1803	432.22	3047	203.58	27.9	27.8 ± 0.14
	1709	428.11		200.53	27.7	
	1778	426.25		204.48	28.0	

3.1.2. Density and Filler Content

The density was measured using Archimedes principle, also known as the buoyancy principle using a Mettler Toledo AX205 DeltaRange balance. Weights were measured in air m_1 and distilled water m_1 with known density ϱ_F. The density ϱ can be calculated by:

$$\varrho = \frac{m_1 \varrho_F}{m_1 - m_2} \tag{2}$$

Three samples of each material were measured and the results are plotted in Figure 3. The materials are ordered and divided into material groups and Aluminum is shown for comparison as commonly used Type III tank liner material. PA and HDPE are the commonly used thermoplastic liner materials. As the results show HDPE has the lowest density and for PA the density depends on the type. As the fillers have a higher density than the thermoplastic matrix (see Table 3 below), density is increased partly significantly, most prominent for the PA6 sample with mineral filler. Regarding the copper coated carbon fibre composites they lead to a high density raise depending on fibre volume content up to the level of aluminum.

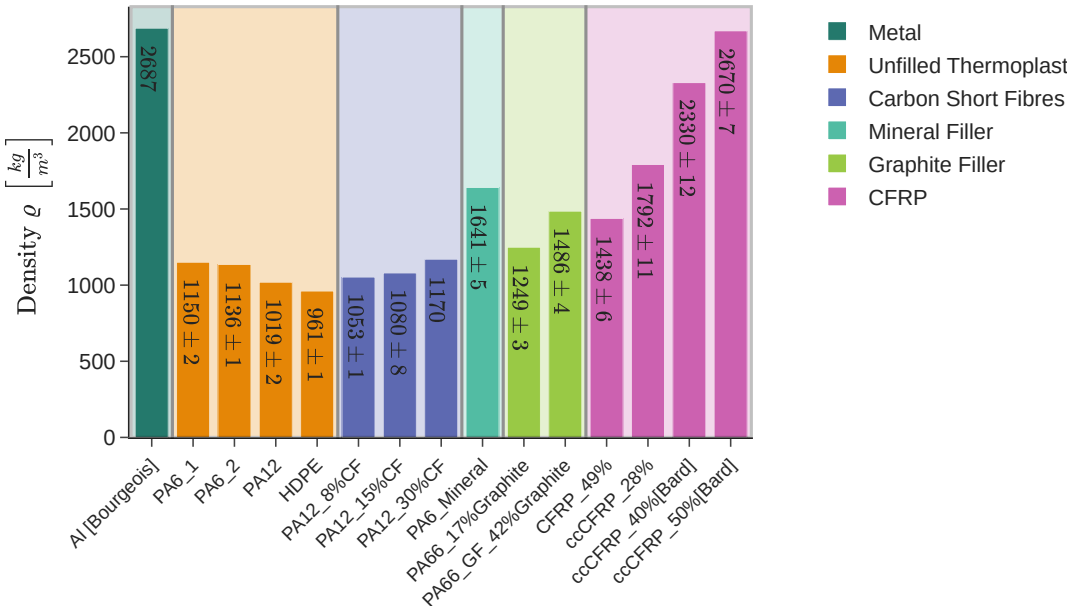

Figure 3. Results of density measurement

The filler mass content Ψ and filler volume content Φ are defined and can be calculated from the measured densities (index F for filler and M for matrix):

$$\Psi = \frac{m_F}{m_F + m_M} = \frac{\varrho_F(\varrho - \varrho_M)}{\varrho(\varrho_F - \varrho_M)} \tag{3}$$

$$\Phi = \frac{V_F}{V_F + V_M} = \frac{\varrho - \varrho_M}{\varrho_F - \varrho_M} = \frac{\varrho}{\varrho_F}\Psi \tag{4}$$

 doi:10.20944/preprints202603.0319.v1

The results are listed in Table 3. The PA66 sample with high graphite content contains also 8%$_{wt}$ glass fibre ($\varrho_{GF} = 2550kg \cdot m^{-3}$ [28]), so the following relation was taken into account to calculate the graphite filler content:

$$\Psi_{GF} = \frac{m_{GF}}{m_F + m_{GF} + m_M} = \frac{8}{100} \tag{5}$$

$$m_{GF} = \frac{2}{23}(m_F + m_M) \tag{6}$$

Table 3. Calculated filler contents from measured densities.

Sample	$\varrho_F \left[\frac{kg}{m^3}\right]$	$\varrho_M \left[\frac{kg}{m^3}\right]$	$\varrho \left[\frac{kg}{m^3}\right]$	Φ [%]	Ψ [%]
PA12_8%CF	1780	1019	1053	4.7	7.6
PA12_15%CF			1080	8.0	13.2
PA12_30%CF			1170	19.8	30.2
PA66_17%Graphite	2200 [4]	1150	1249	9.4	16.6
PA66_GF_42%Graphite			1486	27.0	41.5

3.1.3. Heat Capacity

Heat capacity was measured using dynamic scanning calorimetry (DSC) and the TOPEM method [29], where modulated random temperature pulses are added to the constant temperature rate. By analyzing the phase of the response the heat capacity can be derived. The heat capacity is measured in the range of $0°C \leq T \leq 100°C$ every 1 K using a *Mettler Toledo DSC 2*.

Figure 4 shows the average volumetric heat capacity of three samples per sample material at five chosen temperatures. The volumetric heat capacity c_v is chosen as for comparison in Section 3.2 the same geometry and hence volume is used for all materials. Therefore the volumetric heat capacity is the relevant parameter and is defined by:

$$c_v = c_p \cdot \varrho \left[\frac{J}{m^3 \cdot K}\right] \tag{7}$$

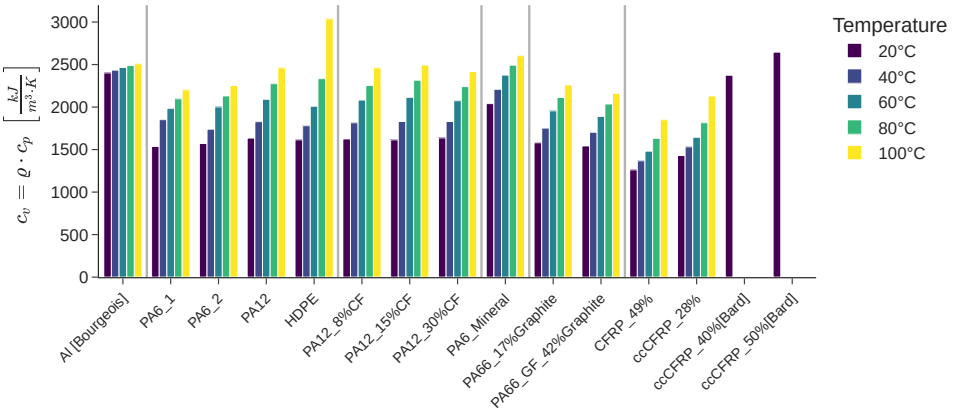

Figure 4. Results volumetric heat capacity (from specific heat and density measurement) at different temperatures

The values published by Bard [26,27] are only available at 20 °C. All materials show a monotonically increasing heat capacity with temperature rise. This effect is most prominent for HDPE, which reaches the overall highest value at 100 °C rendering it as a good candidate as liner material concerning heat absorption. Aluminum shows low temperature dependency and relative high volumetric heat capacity values.

The carbon fibre filled PA12 materials have almost the same values as the unfilled PA12. The mineral filled PA6 shows lower temperature induced growth at high values also at low temperatures, while

 doi:10.20944/preprints202603.0319.v1

graphite reduces the volumetric heat capacity. The CFRP samples have a relatively low volumetric heat capacity, which is increased by fibre volume content of copper coated carbon fibres.

3.1.4. Thermal Conductivity and Temperature Diffusivity

The out-of-plane thermal conductivity $\lambda_\perp \left[W \cdot m^{-1} \cdot K^{-1}\right]$ was characterized using the *Guarded Heat Flow Method (GHFM)* using a *TA Instruments GHFM DTC300* at temperatures $T = \{20, 40, 60, 80\}$ °C. The in-plane and also out-of-plane temperature diffusivities $k_\parallel$ and $k_\perp$ were obtained by the laser flash method (LFA) with a *Netzsch LFA 457 MicroFlash* at the same temperatures as for the GHFM. The in-plane results are not used in the thermal model and hence are not included in this paper. The temperature diffusity and thermal conductivity are related as follows:

$$k = \frac{\lambda}{c_p \cdot \varrho} \left[\frac{m^2}{s}\right] \tag{8}$$

The out-of-plane measurement results are plotted in Figure 5. All materials show decreasing values with increasing temperature. Comparing the two methods the values of the respective samples are generally close by with the exception of *PA66_GF_42%Graphite*. Differences can have numerous causes like laser absorption and infrared emissivity for LFA or bad thermal contact of the samples in GHFM. PA66_GF_42%Graphite shows the highest value. The copper coated carbon fibre composites also show very high thermal diffusivity.

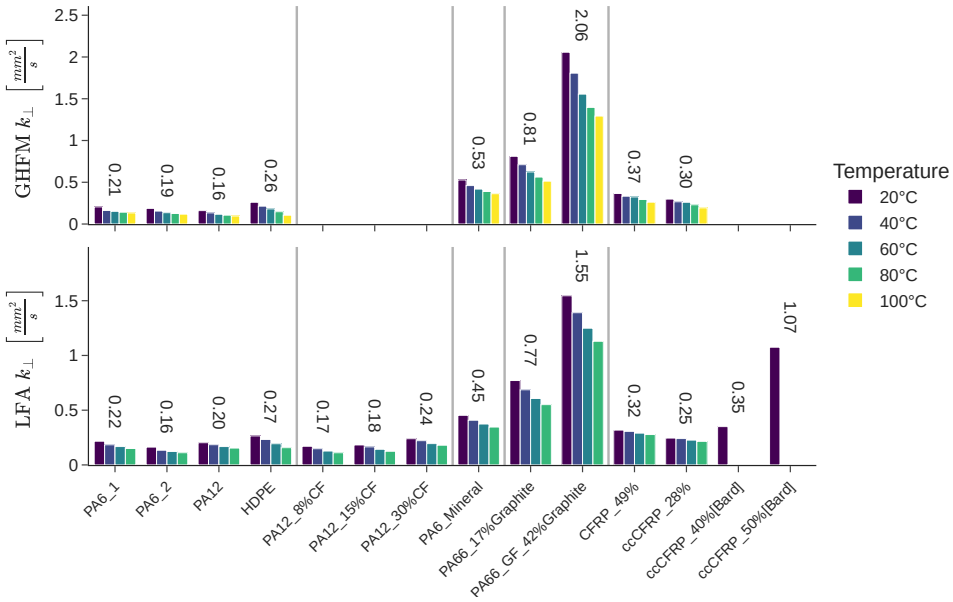

Figure 5. Results temperature diffusivity (top: out-of-plane by guarded heat flow method (derived from thermal conductivity), bottom: out-of-plane by laser flash method.

3.2. Heat Transfer Model

The 1D radial heat transfer equation in cylindrical coordinates is given by [30]:

$$\frac{\partial T}{\partial t} = \frac{1}{r}\frac{\partial}{\partial r}\left(r \cdot k_r \frac{\partial T}{\partial r}\right) + s \tag{9}$$

The explicit finite difference formulation for heterogeneous materials using arithmetic average to calculate the thermal diffusivity between grid points $k_{i+\frac{1}{2}} = \frac{k_i + k_{i+1}}{2}$ is given by [31]:

$$T_i^{n+1} = \frac{1}{2r_i}\frac{\triangle t}{\triangle r^2}\left[(r_i k_i + r_{i+1}k_{i+1})(T_{i+1}^n - T_i^n) - (r_{i-1}k_{i-1} + r_i k_i)(T_i^n - T_{i-1}^n)\right] + T_i^n + s_i^n \triangle t \tag{10}$$

 doi:10.20944/preprints202603.0319.v1

Where the temperature T_i^{n+1} of the next time step t_{n+1} at grid point r_i depends on the temperatures at the current timestep t_n and the surrounding grid points r_{i-1}, r_i, r_{i+1}, the corresponding temperature diffusivity values k_{i-1}, k_i, k_{i+1} and the source term s_i. The spatial grid is evenly spaced with distance Δr into N grid points with grid point index $0 \leq i \leq N-1$ and the time step Δt is constant.

The model scheme is shown in Figure 6. The inner boundary condition was chosen as constant heat flux density to model the released heat during refueling. The magnitude $\dot{q} = 4850\ \frac{W}{m^2}$ was estimated to reach similar end temperatures under comparable model parameters as the results by [13,32,33]. The temperature at the inner border can be calculated by rearranging the energy balance [30]:

$$\dot{q} = -\frac{\lambda_0}{r_0}\frac{T_1 - T_0}{ln\frac{r_1}{r_0}} \quad \Longrightarrow \quad T_0 = T_1 + \frac{\dot{q} r_0 \ln\left(\frac{r_1}{r_0}\right)}{\lambda_0} \tag{11}$$

The outer boundary condition was modeled as convection using a heat transfer coefficient $\alpha = 6\ W \cdot K^{-1} \cdot m^{-2}$ as also used in [13] with an ambient temperature of $T_\infty = 20\ °C$. The outer boundary temperature T_{N-1} can be hence calculated by:

$$\alpha(T_{N-1} - T_\infty) = -\frac{\lambda_{N-1}(T_{N-1} - T_{N-2})}{r_{N-1}\ln\left(\frac{r_{N-1}}{r_{N-2}}\right)} \quad \Longrightarrow \quad T_{N-1} = \frac{T_{N-2}\cdot\lambda_{N-1} + T_\infty \cdot \alpha \cdot r_{N-1}\ln\left(\frac{r_{N-1}}{r_{N-2}}\right)}{\alpha \cdot r_{N-1}\ln\left(\frac{r_{N-1}}{r_{N-2}}\right) + \lambda_{N-1}} \tag{12}$$

Initial temperature was set to $T(t=0) = 20\ °C$. The material properties c_p and k or respectively λ are updated in every time step depending on the current temperature using polynomial fit on measured values. The simulation time was $T_{max} = 180\ s$ with a time step Δt depending on the Courant–Friedrichs–Lewy stability criterion Δt_{crit} [31] $\Delta t = 0.8 \cdot \Delta t_{crit}$:

$$\Delta t = 0.8 \cdot \Delta t_{crit} = 0.8 \cdot \frac{\Delta r^2}{2 \cdot k_{max}} \tag{13}$$

The tank geometry of a previous internal project was used, where the dataset of geometry measurements and burst test are published [34]. The cylindrical area of the tank was chosen for the transient heat transfer calculations with the inner radius of $r_0 = 198\ mm$, liner thickness of $t_{liner} = 8\ mm$ and composite overwrap thickness of $t_{comp} = 26\ mm$ were used with a radial grid spacing of $\Delta r = 0.5\ mm$. The heat transfer model was implemented in *Python*.

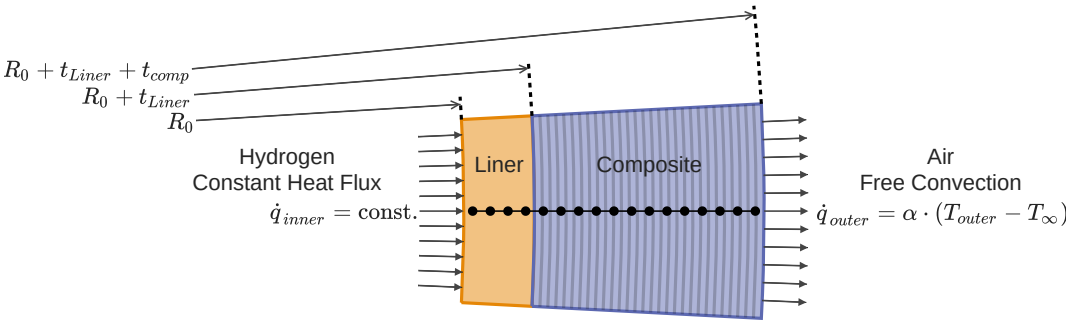

Figure 6. Scheme of the 1D radial finite difference heat transfer model.

Six different material setups were simulated and compared for maximum temperature and weight:

1. *Reference* – PA6 1 liner with standard composite
2. *Reference HDPE* – HDPE liner with standard composite
3. *Reference Type III* – Aluminum liner with standard composite
4. *Mod. Liner* – Modified liner with standard composite
5. *Mod. Composite* – PA6 1 liner with modified composite
6. *Mod. Liner+mod. Composite* – Modified liner and modified composite

 doi:10.20944/preprints202603.0319.v1

7. *Mod. Liner+6 mm mod. Composite* – Modified liner with 6 mm modified composite and 20 mm standard composite

PA6 and HDPE were chosen as reference liner materials as modified liner the material data of *PA66_GF_42%Graphite* was used. For the standard composite the data of *CFRP_49%* and for the modified composite the data of *ccCFRP_50%[Bard]* was used.

In Figure 7 the simulation results of the reference Type IV tank and the tank with modified liner and modified composite overwrap is shown. The top plots show the temperature profile after 180 s over the wall thickness and the bottom plots show the temperature evolution over time using a color representation. The thermal simulation of the reference tank show a maximum temperature of 108.2 $°C$ at the inner liner surface with a steep temperature gradient inside the liner, while at the outer surface the heat-up is negligible. The results of the modified liner and modified composite reveal that the maximum temperature of 54.3 $°C$ is significantly lower and the composite structure absorbed more heat. The outer boundary temperature of 24.2 $°C$ is still low, hence the heat transfer into the surrounding negligible for very fast filling, as also other studies showed [13,32].

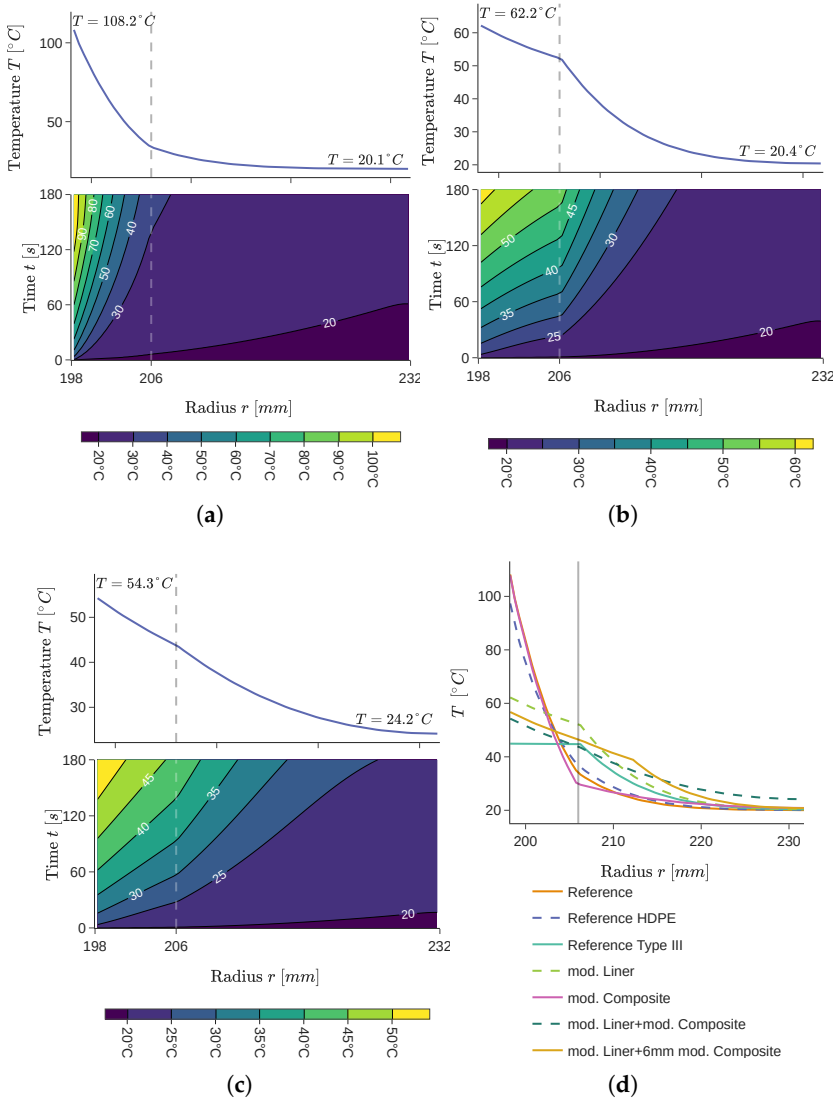

Figure 7. Comparison of simulation results (for (**a**) - (**c**) top: temperature profile over radius at end of refueling, bottom: contour plot of temperature evolution over radius): (**a**) Reference of PA6 liner and composite overwrap. (**b**) Modified liner (*PA66_GF_42%Graphite*) and composite overwrap. (**c**) Modified liner (*PA66_GF_42%Graphite*) and modified composite overwrap (*ccCFRP_50%[Bard]*). (**d**) Temperature profile over radius at end for all material setups.

 doi:10.20944/preprints202603.0319.v1

The simulation results are compared in Figure 8 showing the maximum temperature and weight per cylinder length. The results show that from a thermal perspective HDPE is a better suited liner material as PA6 leading to a maximum temperature reduction of 10.8 K by even reducing the weight by 2.8 %. The Type III tank with aluminum liner achieves the lowest temperature while weighing 25.0 % more (assuming the same thickness as for Type IV).

Using the modified liner material *PA66_GF_42%Graphite* while using the standard composite overwrap the temperature peak is lowered significantly by 63.3 K leading to a weight increase of 5.6 %. Modifying only the composite results in almost no thermal improvement, but in a weight increase of 70%. During the short refueling time the bottle neck is the thermoplastic liner and hence the heat is not transfered into the overwrap. Using modified material for both the liner and the overwrap the temperature can be decreased more compared to only modifying the liner, but comes at a high weight increase. Finally using only modified composite material for the first 6 mm of the overwrap the temperature is lowered further than only modifying the liner.

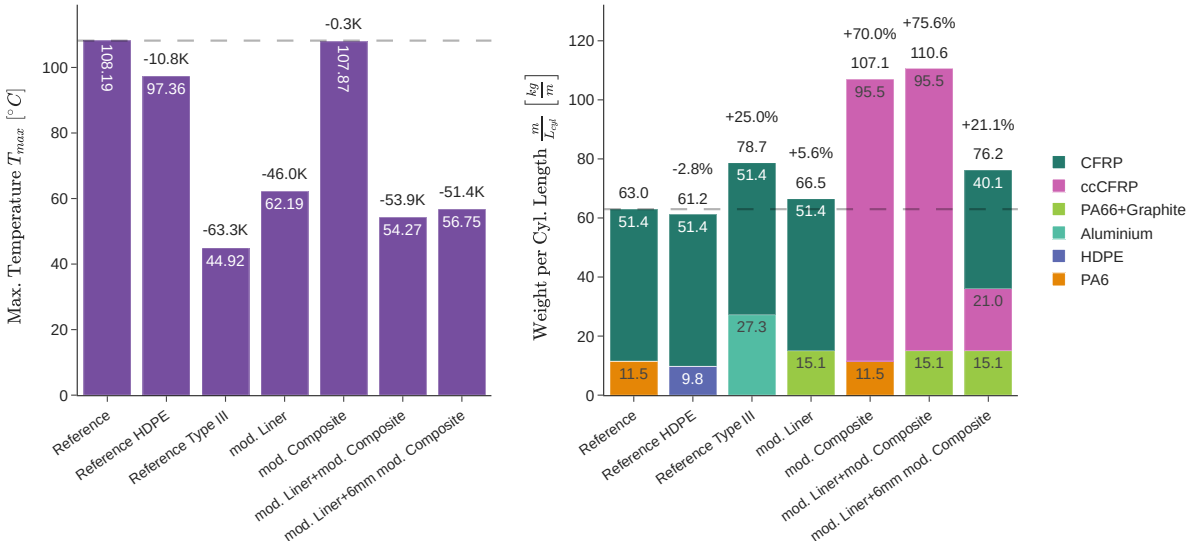

Figure 8. Summary of simulation results of different material combinations (left: Maximum temperature after 180 s refueling, right: Weight per cylinder length).

4. Discussion

A simplified approach using only a 1D thermal model was used to compare different material combinations to estimate the potential in improving the transfer of the heat released during hydrogen refueling and to decrease the peak temperature. Literature review of CFD simulations and experiments regarding the heat development of hydrogen refueling [9,12–14,16–18] showed that in many cases due the high fluid velocity and turbulent flow the heat is nearly evenly distributed. This means that a 1D radial heat model is a good first estimation to, while neglecting the influence of different local composite stacking and thicknesses and also of the metallic nozzle. Future studies are planned to take those effects into account using a 3D heat model.

As described in Section 3.1.1 due to a low fibre volume content of the composite sample with copper coated carbon fibres, material properties taken from literature had to be used for the thermal model. This introduces uncertainties regarding the comparability of the cited and the acquired properties as the measurement methods differ. Also the cited values are only available at 20 °C, while the heat capacity increases and the temperature diffusivity decreases with increasing temperature for all characterized materials. Thus the quantitative accuracy of the model is limited, but it is not expected to have a significant influence of the overall outcome that modifying the liner material has the highest potential to reduce the peak temperature while only introducing little weight gain and modification of the standard configuration.

 doi:10.20944/preprints202603.0319.v1

Modifying the liner by using PA6 filled with graphite seems to be the best option to improve heat transfer and absorption during refueling. The weight increase is marginal while having a very positive effect on the heat transfer. Additionally it has been shown that graphite reduces hydrogen permeability [4] which might also allow a reduction of liner thickness. The composite overwrap can remain as is, so the impact of the modification like mechanical strength is expected to be low and can facilitate certification. If only the liner has to be modified, the cost increase is expected low compared to the overall tank manufacturing cost. A possible risk of higher costs is the manufacturability of liners using the modified thermoplastic e.g. by rotary molding due to the lag of experience with this kind of materials.

The presented passive means for improved heat transfer during hydrogen refueling can help to reduce refueling times, to reach higher states of charge and to decrease the need for pre-cooling.

Future studies will concentrate on other tank designs like a hybrid Type IV/V tank where the liner is melted under temperature and partly infused into the wound carbon fibres forming a thermoplastic interface before the remaining dry fibres are inmpregnated with a thermoset matrix [7,35]. This design is expected to lead to better thermal contact and also reduces the heat transfer path length. Future research will also include experimental refueling tests on modified tanks with structure integrated of temperature sensors in order to monitor the temperature gradient.

5. Conclusions

The results show that the modification of PA6 as commonly used liner material using a graphite filler can significantly decrease the peak temperature during fast hydrogen refuelling, showing that the liner is the bottleneck. The peak temperature was reduced by 46.0 K while increasing the weight by 5.6 %. The effect of modifying the composite overwrap using copper coated carbon fibres is only minor while the weight gain is relatively high.

The prepared composite samples for this study only achieved low fibre volume content resulting in the need to use thermal properties from literature limiting the model accuracy. Additionally the study only uses a radial 1D thermal neglecting tank inhomogeneities for a first comparison of material combinations as a preselection of future research using more detailed models and experiments.

Author Contributions: Conceptualization, N.L. and S.R.; methodology, N.L. and S.R.; software, N.L.; validation, N.L.; formal analysis, N.L.; investigation, N.L. and S.R.; data curation, N.L. and S.R.; writing—original draft preparation, N.L.; writing—review and editing, N.L: and S.R.; visualization, N.L.; supervision, N.L. and S.R.; project administration, N.L. and S.R. All authors have read and agreed to the published version of the manuscript.

Funding: This research received no external funding.

Data Availability Statement: Data is available upon request.

Acknowledgments: The authors would like to thank Hendrik Lange for carrying out a part of the experiments and measuements. Furthermore the authors thank MOCOM for providing samples.

Conflicts of Interest: The authors declare no conflicts of interest.

Abbreviations

The following abbreviations are used in this manuscript:

COPV	Composite Overwrapped Pressure Vessels
CF	Carbon Fibre
CFRP	Carbon Fibre Reinforced Plastic
ccCFRP	CFRP with Copper Coated Carbon Fibres
SOC	State of Charge
FVC	Fibre volume content
DSC	Differential scanning calorimetry

 doi:10.20944/preprints202603.0319.v1

TGA	Thermogravimetric analysis
PA	Polyamide
HDPE	High-Density Polyethylen

References

1. Liebers, N.; Ropte, S. Accelerated refueling of type IV hydrogen pressure tanks by passive means: Thermal material characterization and evaluation. In Proceedings of the EASN 2025, Madrid Spain.
2. Penavayre, C.; Fitoussi, J.; Richaud, E.; Papin, P.; Bouneb, J.; Hochstetter, G.; Shirinbayan, M. Long–Term Behavior of Carbon Fiber–Reinforced Thermoplastic Composites for Type V Hydrogen Storage Tanks: Effects of Hygrothermal Aging on Physicochemical and Mechanical Properties. *Polymer Composites* **2025**. https://doi.org/10.1002/pc.70229.
3. Barthelemy, H.; Weber, M.; Barbier, F. Hydrogen storage: Recent improvements and industrial perspectives. *International Journal of Hydrogen Energy* **2017**, *42*, 7254–7262. https://doi.org/10.1016/j.ijhydene.2016.03.178.
4. Rosen, P.A. Beitrag zur Optimierung von Wasserstoffdruckbehältern. Dissertation, Technische Universität Chemnitz, 2017.
5. Su, Y.; Lv, H.; Zhou, W.; Zhang, C. Review of the Hydrogen Permeability of the Liner Material of Type IV On-Board Hydrogen Storage Tank. *World Electric Vehicle Journal* **2021**, *12*, 130. https://doi.org/10.3390/wevj12030130.
6. Muthukumar, P.; Kumar, A.; Afzal, M.; Bhogilla, S.; Sharma, P.; Parida, A.; Jana, S.; Kumar, E.A.; Pai, R.K.; Jain, I.P. Review on large-scale hydrogen storage systems for better sustainability. *International Journal of Hydrogen Energy* **2023**, *48*, 33223–33259. https://doi.org/10.1016/j.ijhydene.2023.04.304.
7. Büchner, K. Pilotstudie zur Herstellung von Wasserstoff-Hochdrucktanks mittels thermoplastischer Radialtränkung der Faserwicklung. Masterarbeit, Otto-von-Guericke-Universität, Magdeburg, 2023.
8. Liu, Y.L.; Zhao, Y.Z.; Zhao, L.; Li, X.; Chen, H.g.; Zhang, L.F.; Zhao, H.; Sheng, R.H.; Xie, T.; Hu, D.H. Experimental studies on temperature rise within a hydrogen cylinder during refueling. *International Journal of Hydrogen Energy* **2010**, *35*, 2627–2632. https://doi.org/10.1016/j.ijhydene.2009.04.042.
9. Li, M.; Bai, Y.; Zhang, C.; Song, Y.; Jiang, S.; Grouset, D.; Zhang, M. Review on the research of hydrogen storage system fast refueling in fuel cell vehicle. *International Journal of Hydrogen Energy* **2019**, *44*, 10677–10693. https://doi.org/10.1016/j.ijhydene.2019.02.208.
10. *Regulation No 134 of the Economic Commission for Europe of the United Nations (UN/ECE) — Uniform provisions concerning the approval of motor vehicles and their components with regard to the safety-related performance of hydrogen-fuelled vehicles (HFCV) [2019/795]*; 2019.
11. Fuel Cell Standards Committee. Standard for Fuel Systems in Fuel Cell and Other Hydrogen Vehicles. https://doi.org/10.4271/J2579{_}202301.
12. Blanco-Aguilera, R.; Martinez-Agirre, M.; Berasategi, J.; Penalba, M.; Bou-Ali, M.M.; Shevtsova, V. Effect of liner thermal properties and liner pre-cooling on the thermal management of fast-filling of hydrogen tanks. *International Journal of Hydrogen Energy* **2024**, *52*, 1159–1172. https://doi.org/10.1016/j.ijhydene.2023.06.285.
13. Bourgeois, T.; Brachmann, T.; Barth, F.; Ammouri, F.; Baraldi, D.; Melideo, D.; Acosta-Iborra, B.; Zaepffel, D.; Saury, D.; Lemonnier, D. Optimization of hydrogen vehicle refuelling requirements. *International Journal of Hydrogen Energy* **2017**, *42*, 13789–13809. https://doi.org/10.1016/j.ijhydene.2017.01.165.
14. Melideo, D.; Baraldi, D. CFD analysis of fast filling strategies for hydrogen tanks and their effects on key-parameters. *International Journal of Hydrogen Energy* **2015**, *40*, 735–745. https://doi.org/10.1016/j.ijhydene.2014.10.138.
15. Melideo, D.; Baraldi, D.; Galassi, M.C.; Ortiz Cebolla, R.; Acosta Iborra, B.; Moretto, P. CFD model performance benchmark of fast filling simulations of hydrogen tanks with pre-cooling. *International Journal of Hydrogen Energy* **2014**, *39*, 4389–4395. https://doi.org/10.1016/j.ijhydene.2013.12.196.
16. Wang, X.; Tian, M.; Chen, X.; Xie, P.; Yang, J.; Chen, J.; Yang, W. Advances on materials design and manufacture technology of plastic liner of type IV hydrogen storage vessel. *International Journal of Hydrogen Energy* **2022**, *47*, 8382–8408. https://doi.org/10.1016/j.ijhydene.2021.12.198.
17. WOODFIELD, P.L.; Monde, M.; Takano, T. Heat Transfer Characteristics for Practical Hydrogen Pressure Vessels Being Filled at High Pressure. *Journal of Thermal Science and Technology* **2008**, *3*, 241–253. https://doi.org/10.1299/jtst.3.241.
18. Kim, S.C.; Lee, S.H.; Yoon, K.B. Thermal characteristics during hydrogen fueling process of type IV cylinder. *International Journal of Hydrogen Energy* **2010**, *35*, 6830–6835. https://doi.org/10.1016/j.ijhydene.2010.03.130.

 doi:10.20944/preprints202603.0319.v1

19. Wieme, T.; Duan, L.; Mys, N.; Cardon, L.; D'hooge, D.R. Effect of Matrix and Graphite Filler on Thermal Conductivity of Industrially Feasible Injection Molded Thermoplastic Composites. *Polymers* **2019**, *11*. https://doi.org/10.3390/polym11010087.
20. Travaš, L.; Rujnić Havstad, M.; Pilipović, A. Optimization of Thermal Conductivity and Tensile Properties of High-Density Polyethylene by Addition of Expanded Graphite and Boron Nitride. *Polymers* **2023**, *15*. https://doi.org/10.3390/polym15173645.
21. Tavman, I.H. Thermal and mechanical properties of copper powder filled poly (ethylene) composites. *Powder Technology* **1997**, *91*, 63–67. https://doi.org/10.1016/S0032-5910(96)03247-0.
22. Patnaik, A.; Abdula, M.; Biswas, S.; Satapathy, A. Thermal conductivity of particulate filled polymer composites. *Materials Science : an Indian Journal (MSAIJ)* **2009**, *5*, 306–318.
23. Grundler, M.; Derieth, T.; Heinzel, A. Polymer compounds with high thermal conductivity. Author(s), 2016, AIP Conference Proceedings, p. 030015. https://doi.org/10.1063/1.4965485.
24. Chen, H.; Ginzburg, V.V.; Yang, J.; Yang, Y.; Liu, W.; Huang, Y.; Du, L.; Chen, B. Thermal conductivity of polymer-based composites: Fundamentals and applications. *Progress in Polymer Science* **2016**, *59*, 41–85. https://doi.org/10.1016/j.progpolymsci.2016.03.001.
25. Che, J.; Wu, K.; Lin, Y.; Wang, K.; Fu, Q. Largely improved thermal conductivity of HDPE/expanded graphite/carbon nanotubes ternary composites via filler network-network synergy. *Composites Part A: Applied Science and Manufacturing* **2017**, *99*, 32–40. https://doi.org/10.1016/j.compositesa.2017.04.001.
26. Bard, S. Kohlenstofffaser-Epoxydharz-Verbunde mit erhöhter Wärmeleitfähigkeit: Struktur und Eigenschaften. Dissertation, Universität Bayreuth, Bayreuth, 2021.
27. Bard, S.; Schönl, F.; Demleitner, M.; Altstädt, V. Copper and Nickel Coating of Carbon Fiber for Thermally and Electrically Conductive Fiber Reinforced Composites. *Polymers* **2019**, *11*. https://doi.org/10.3390/polym11050823.
28. Schürmann, H. *Konstruieren mit Faser-Kunststoff-Verbunden*, 2., bearb. und erw. aufl. ed.; Springer: Berlin, 2007.
29. Mettler Toledo. TOPEM® – the new advanced multi-frequency TMDSC technique.
30. VDI-Gesellschaft Verfahrenstechnik und Chemieingenieurwesen., Ed. *VDI-Wärmeatlas: Mit 320 Tabellen*, 11., bearb. und erw. aufl. ed.; VDI/-Buch], Springer Vieweg: Berlin and Heidelberg, 2013.
31. Langtangen, H.P. *Finite difference computing with PDEs: A modern software approach*; Vol. vol. 16, *Texts in computational science and engineering*, Springer Open: Cham Switzerland, 2017. https://doi.org/10.1007/978-3-319-55456-3.
32. Monde, M.; Woodfield, P.; Takano, T.; Kosaka, M. Estimation of temperature change in practical hydrogen pressure tanks being filled at high pressures of 35 and 70 MPa. *International Journal of Hydrogen Energy* **2012**, *37*, 5723–5734. https://doi.org/10.1016/j.ijhydene.2011.12.136.
33. Couteau, A.; Dimopoulos Eggenschwiler, P.; Jenny, P. Heat transfer analysis of high pressure hydrogen tank fillings. *International Journal of Hydrogen Energy* **2022**, *47*, 23060–23069. https://doi.org/10.1016/j.ijhydene.2022.05.127.
34. Lüders, C.; Ropte, S.; Schmidt, D.; Liebisch, M. Dataset on hydraulic burst pressure test of Type IV composite pressure vessel. *Data in brief* **2025**, *59*, 111333. https://doi.org/10.1016/j.dib.2025.111333.
35. Ropte, S. Verfahren und Werkzeug zur Herstellung eines Faserverbund-Hohlkörpers. DE102022103036, 2022.